A Submillipound Mercury Electron Bombardment Thruster

PAUL D. READER,* SHIGEO NAKANISHI,† WALTER C. LATHEM,†
AND
BRUCE A. BANKS†
NASA Lewis Research Center, Cleveland, Ohio

Several similar 5-cm-diam electron bombardment ion thrusters and tests used to improve the performance of the thruster components are discussed. Cathode pole piece and baffle position and geometry significantly influence ion chamber performance and are used to tailor the discharge characteristics to obtain desired operational modes. Both chamber and neutralizer emitters are enclosed hollow cathode types. The chamber cathode operates on the total flow through the discharge chamber. The neutralizer cathode has been operated successfully at mercury flow rates below 2 ma of equivalent flow while coupled to an operating thruster beam. All thruster tests were conducted with single, glass-coated grids. Tests of glass-coated grids designed to provide single and multiple axis electrostatic thrust vectoring resulted in electrical shorts between elements caused by sputtered material from the tank. A thruster system design resulting from the above component tests is described. Over-all thruster efficiencies of 20% at a specific impulse of 1800 sec have been demonstrated at a thrust level of 0.36 mlb.

Introduction

SPACECRAFT in operation today have demonstrated impressive gains in reliability and useful life over those launched during the early 60's. Future orbiting spacecraft with design lifetimes of several years place severe requirements on attitude control and stationkeeping subsystems. The long life and high specific impulse available from low thrust, electrostatic thruster systems makes them increasingly competitive for these functions. Thrust levels in the submillipound range, for example, are of particular interest for spacecraft in the 1000–2000 lb class.[1,2]

This paper presents the results of component tests of several 5-cm-diameter mercury electron bombardment ion thrusters. Ion chamber and magnetic field variations are described. Results with enclosed hollow cathodes used for both the main chamber and the neutralizer emitters are presented and compared with open hollow cathodes of the type flown on Space Electric Rocket Test II (SERT II).[3] All thruster tests were conducted with single, glass-coated accelerator grids.[4] Accelerator grid fabrication techniques and several grid designs (including vectorable grids) are described. Finally, a thruster system design resulting from these component tests is detailed. Some spacecraft applications possible with this thruster system are then considered.

The vacuum facility used for this investigation was 4.5 m long by 1.5 m in diameter. The thruster test chamber was connected to the facility through a 0.3 m gate valve. A stainless steel tank divider limited the ion beam length to 2 m. The facility was maintained at 10^{-6} torr during thruster operation. Details on the facility are found in Ref. 5.

Discharge Chamber

A cross section of the thruster discharge chamber used for research tests is shown in Fig. 1. Five different lengths were tested by substituting different length chamber shell and anode sections.

The conical cathode pole piece has screen-covered holes in its sides to allow mercury from the cathode to flow radially into the discharge chamber. The diameter and location of the downstream end of the cathode pole piece were scaled from SERT II. The conical shape was necessary to provide cathode clearance. The baffle was kept at the plane of the downstream surface of the conical pole piece for all tests, but the shape was varied. Full cover baffles with various hole sizes in the center and centrally located disc baffles of different diameters were tested. The discs were suspended by 3 wires, 120° apart attached to the pole piece. The magnetic field strength was varied by changing the number of rod magnets.

In addition to these changes, ranges of neutral flow rates and voltages were tested. Precision 0.5 mm bore glass tubing was used as propellant reservoirs for the research runs to allow accurate mercury flow rate measurements. Figure 2 shows the effect of net accelerating voltage variations on discharge chamber losses per beam ion (ev/ion) for three chamber lengths studied. (The glass-coated grid used for these tests is described later.) As net accelerating voltage was increased, a marked improvement in discharge efficiency (lower ev/ion) resulted for the three chamber lengths shown. The discharge losses decreased by more than a factor of two as the chamber was shortened from 6.67 cm to 4.76 cm. The 4.76-cm-long chamber was best and operated with primary discharge losses of 110 ev/ion at a net accelerating potential of 650 v.

Individual changes in magnetic field, pole piece baffle configuration and propellant utilization efficiency were also made;

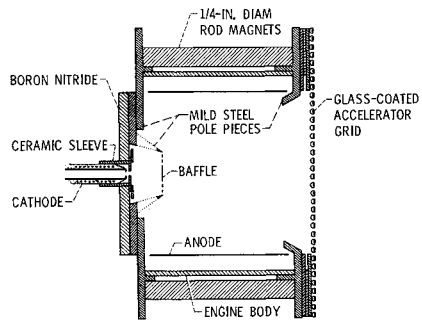

Fig. 1 Cross section of 5-cm-diam thruster discharge chamber.

Presented as Paper 70-616 at the AIAA 6th Propulsion Joint Specialist Conference, San Diego, Calif., June 15–19, 1970; submitted July 6, 1970; revision received August 10, 1970.

* Head, Propulsion Components Section. Member AIAA.

† Aerospace Research Engineer.

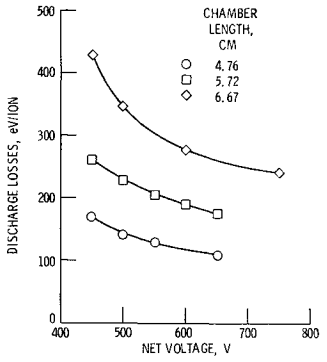

Fig. 2 Effect of net accelerating voltage on discharge chamber losses for three ion chamber lengths with 34–36 v discharges, 70% propellant utilization efficiency, and 30 ma beam current.

however, the chamber length was found to be the dominant factor in improving thruster performance as shown in Fig. 3. The curves are lines of constant discharge energy loss per beam ion produced. They are shown to allow discharge efficiency comparisons between configurations having operating points at different discharge currents and voltages. The data points associated with a particular chamber length fall roughly along lines of constant discharge energy loss per beam ion. The data scatter in each case is mainly due to the effects of baffle shape, magnetic field strength, and propellant utilization efficiency. Baffles with central holes and high magnetic field strengths increased discharge voltage, while disc baffles and moderate field strengths lower the voltage. Operation at higher propellant utilization efficiency required lower propellant flow rates at a constant beam current resulting in a lower density, higher voltage discharge characteristic.

In the range of discharge voltage between 20 and 40 v the discharge performance improved with decreasing chamber length for a number of other parametric changes. The 4.76-cm-long chamber operated at discharge losses below 200 ev/ion. A 3.75-cm-length chamber was briefly tested and exhibited very unstable operation with higher discharge losses. Further optimization tests are being conducted on magnetic field and baffle configurations using the 4.76-cm-long chamber.

At the 110 ev/ion point previously mentioned, only 3.4 w were consumed in the primary chamber discharge, but 7 w (or about 230 ev/ion were lost in the cathode keeper discharge. Thus, for small thrusters several power losses become of the same magnitude as ionization losses. The ionization losses are therefore more representative of thruster performance for larger thrusters than for smaller thrusters.

Cathodes

Main Cathodes

The two types of hollow cathodes used in this program are shown in Fig. 4. The SERT II type, or open hollow cathode, is shown in Fig. 4a. Mercury vapor flows into a 0.32-cm-diam tantalum tube closed at one end except for a small aperture in a 2% thoriated tungsten tip. An insert coated with barium carbonate aids the initiation of a cathode discharge and generally improves cathode emission. The cathode tip is

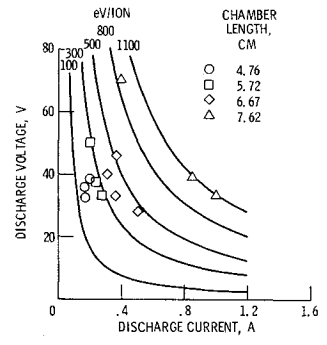

Fig. 3 Discharge chamber current voltage relationship for four chamber lengths; beam current was 30 ma, net accelerating voltage 450 v, and total extraction voltage 675 v.

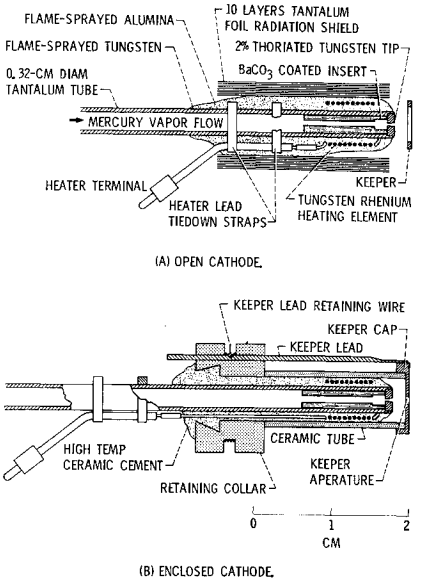

Fig. 4 Comparison of open (SERT II) and enclosed hollow cathodes configuration.

heated electrically by an encapsulated tungsten-rhenium heater element. The cathode discharge is started by heating the cathode tip and applying about 300 v potential between the cathode and the keeper. The keeper is a 4.8-mm inside diameter ring fabricated of 1.52-mm wire. The ring is 1.5-mm downstream of the cathode orifice.

A cutaway sketch of the enclosed cathode type is shown in Fig. 4b. The changes made to the open cathode were done in an attempt to minimize discharge coupling voltage effects and radiated heat losses. Also of equal importance is the fact that the integrated construction provides positive spacing and alinement of the keeper electrode. The tantalum keeper cap was 0.25 mm thick with a 3.2-mm-diam aperture. The keeper was positioned 1.5 mm from the cathode aperture by means of a ceramic tube over the cathode body. A ceramic retaining collar cemented to the cathode body held the keeper and tube in the proper relative positions. Disassembly was accomplished easily by removing the keeper lead retaining wire.

Figure 5 shows a comparison of data taken with the open and enclosed cathodes at the same thruster operating condi-

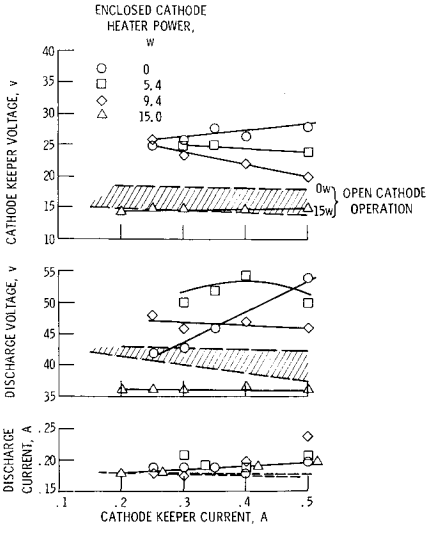

Fig. 5 Ion chamber and cathode characteristics with net accelerator voltage of 650 v, propellant utilization efficiency of 68%, and propellant flow rate of 42 ma.

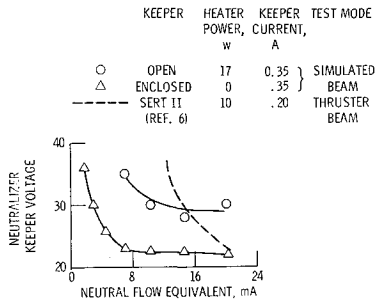

Fig. 6 Keeper discharge characteristics of neutralizers.

tions. The open cathode operation bands are shown shaded and the enclosed cathode data are shown as symboled curves.

With the open cathode the chamber discharge current and voltage and cathode keeper voltage were nearly constant for keeper currents between 0.2 and 0.5 amp as the cathode heater power was dropped from 16 to 5 and finally 0 w. One variation from this condition was an instability which developed at keeper currents below 0.25 amp when the open cathode was at zero heater power. Enclosed cathode operation at similar powers showed a wider range of keeper voltage, discharge voltage, and discharge current.

From these data it was concluded that either hollow cathode could satisfy the main chamber cathode requirements. Cathode heat losses can be reduced while maintaining the necessary cathode temperature by using improved shielding and insulating techniques. The enclosed cathode demonstrated greater stability over a wider range of discharge chamber variables than the open cathode and is of greater interest because of its structural integrity.

Neutralizer

The operating requirements for the neutralizer are low neutral propellant flow, minimum heating power, and low beam coupling voltage. Enclosed and open cathodes, identical in design to those described in the previous section (Fig. 4), were tested for use as neutralizers.

The effect of neutralizer flow upon keeper voltage of the open and enclosed configurations tested with a simulated beam is shown in Fig. 6. The date from Ref. 6 for the SERT II neutralizer operating with a thruster system are also shown on the figure as a dashed curve. The open and enclosed cathodes were tested by starting a discharge to a collector anode to simulate thruster operation. Both the open keeper and the SERT II configurations were operated with heater power while the enclosed keeper was not. With the open keeper, the keeper voltage began to rise sharply at a flow rate of about 8 ma equivalent neutral flow. The keeper discharge ceased to operate below about 6 ma of neutral flow. The differences in

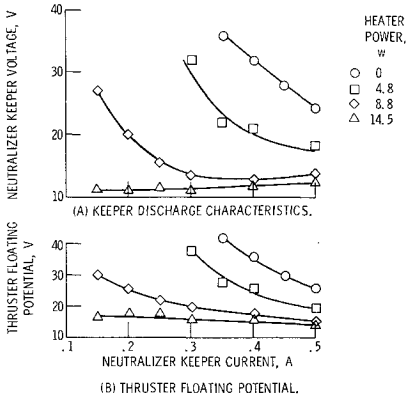

Fig. 7 Neutralizer discharge characteristics of reduced size (⅔ SERT II diam) enclosed cathode with ion beam current of 0.030 A, net accelerating voltage of 650 v, and neutralizer flow rate of 2.25 ma.

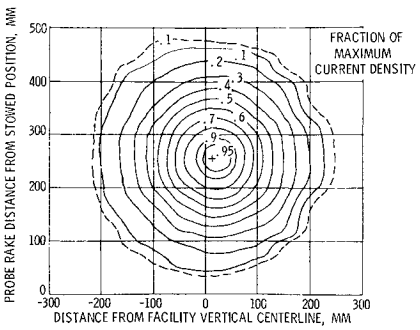

Fig. 8 Beam current density contour map taken with punched molybdenum grid at 600 net accelerating voltage; dash curve from 450 v point.

the open keeper and SERT II keeper discharge characteristics may be due to the difference in heater power levels.

The neutralizer cathode with the enclosed keeper was operated with no heater power, a stringent condition which should give less optimistic results than operation with heater power. The keeper discharge operated successfully down to neutral flows of less than 2 ma. On the basis of required neutral flow, the enclosed keeper hollow cathode is superior to the open cathode for neutralizer operation on a 5-cm thruster.

A smaller diameter version of the enclosed hollow cathode was fabricated of 0.203-cm outside diameter tantalum tube and tested on a 5-cm thruster. All other cathode design features were essentially unchanged. Preliminary results are shown in Fig. 7. At zero heater power and 0.35 amp keeper current the keeper voltage was approximately equal to that obtained for simulated beam operation (see Fig. 6). This supports the viewpoint that simulated beam tests of neutralizers are valid and also suggests that a reduction in cathode outside diameter had no effect on performance. With the application of heater power, lower neutralizer keeper voltages were possible at a given value of keeper current.

The variation in thruster floating potential with neutralizer keeper current for the four levels of heater power is shown in Fig. 7b. As noted above, the trend observable in the keeper voltage was reflected in the floating potential.

Satisfactory neutralization has been obtained with an enclosed hollow cathode at neutral flow rates as low as 2.25 ma. Sufficient electron emission for neutralization at low heater power appears feasible with further improvements in thermal design.

Accelerator Grid Fabrication and Performance

Both composite and double grid systems have been tested on 5-cm diam thrusters.[7,8] The results of Ref. 8 showed that the discharge power loss was reduced by about one half when a double grid system was replaced by a glass-coated or composite grid. All of the grid system tests discussed in this paper were conducted with composite grids.

Nonvectorable Grids

The grid used for the discharge chamber studies was a 0.38-mm- thick punched molybdenum sheet having a hex-

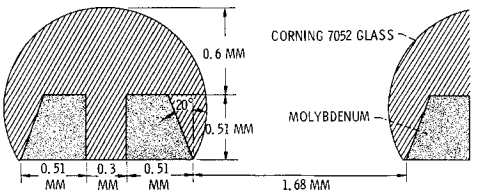

Fig. 9 Cross-sectional geometry of typical element set of glass coated electric discharge machined quadrant vector grid.

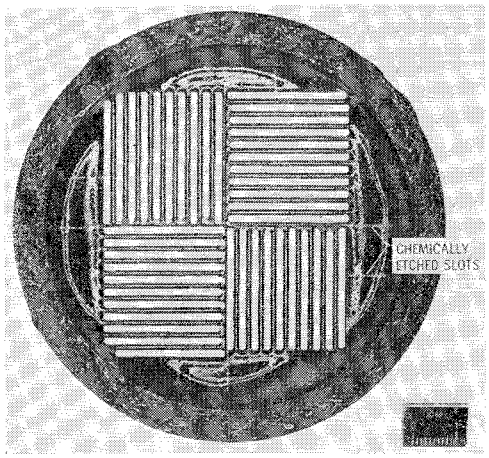

Fig. 10 Coated side of quadrant vector grid showing peripheral support ring.

agonal array of 1.91-mm-diam holes. The glass-coated side was covered by 0.57-mm-thick Corning 7052. The glass coating also covers the hole walls so that the actual coated hole inside diameter is 1.38 mm. The grid was fabricated according to the process described in Ref. 4.

A molybdenum button rake system was used to obtain current density profile measurements with this grid. Fifteen 1.27-cm-diam molybdenum disks were spaced along the 51-cm rake. The rake was located 58.4 cm downstream of the accelerator grid and traversed 40.6 cm across the ion beam.

The ion beam profile measuring the processing equipment is described in detail in Ref. 9. The currents measured at the molybdenum buttons were processed on a digital computer, and the results were stored on magnetic tape. Further computer processing yielded microfilm plots showing two-dimensional contour maps of equal current density, coordinates of the centroid of the distribution and an integrated value of beam current.

Figure 8 shows a typical contour plot made from probe rake measurements. The dashed contour is a 0.1 maximum current density contour taken with the same grid operating at a lower accelerating voltage. The beam divergence half-angle represented by the dashed curve is 20°.

Over 200 hr of testing have been accomplished with the grid used to make these measurements without visible deterioration to the grid. Accelerator drain currents have been less than 1% of the beam current.

Vectorable Grids

Thrust vectoring systems which operate without the use of moving parts are desirable. Several electrostatic thrust vectoring grid designs were investigated and will be briefly discussed.

A two-dimensional aperture grid consisting of parallel bars of molybdenum was designed to provide vectoring capability in two orthogonal directions. A cross section of a typical element set is shown in Fig. 9 and the coated grid is shown in Fig. 10. The grid was fabricated by electric discharge machining. The grid geometry was designed so as to provide support and positive separation of elements during fusing of the glass to the grid. This grid was repeatedly slurry sprayed and fired with Corning 7052 glass until a thickness of approximately 0.6 mm was achieved. The final firing of the grid consisted of fusing a molybdenum ring to the periphery of the grid. This ring provides both additional mechanical support to the grid and electrically isolated mounting.

Thin slots in the molybdenum periphery shown in Fig. 10 were electrochemically machined away to provide four electrically isolated quadrants and one common set of conductor elements that interlace each of the four quadrants. The quadrants were electrically connected to provide deflection in the same direction from diametrically opposing quadrants. Preliminary tests of this grid indicated that the interlacing combs of elements could support accelerator potentials differences of over 100 v. However, after only a few minutes of thruster operation an accumulation of back-sputtered metal on the downstream surface of glass between the conductors caused shorting of the interlacing combs. The rapid buildup of conducting sputtered metal, which caused shorting of the grid electros, appears to be a facility testing problem because of back-sputtered material from vacuum facility walls and target. Sputtered material from the thruster ground screen, neutralizer, or from the downstream face of the grid itself may also have contributed to the problem, but can be overcome by appropriate design. Close inspection of the upstream face of the grid showed a very thin glass coating covering two areas near the grid center. These areas suffered electrical breakdown and direct ion impingement while the grid was operating on the thruster. Figure 11 is a beam current density contour map taken of the quadrant grid operating with all elements at the same potential. The four current density peaks shown in Fig. 12 result from the overlapping of the beams from each quadrant. (A two-dimensional aperture produces a fan beam with the greater spread normal to the long aperture dimension.)

One method to eliminate the local thin spots on grid glass coating is to make the single conductor elements much wider so that they appear similar to the double conductor elements. A grid of this design, coated with Corning 1723 glass was fabricated and tested. This grid was capable of sustaining high voltage, and higher beam currents (35 ma) were possible, but again back-sputtered material from the facility resulted in shorting of the parallel conductors.

In another approach to a vectorable grid design, a method of fusing two molybdenum wires to Corning 7052 cane was

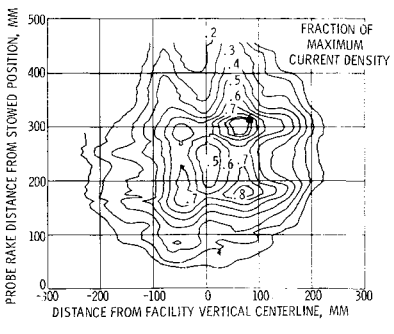

Fig. 11 Beam current density contour map taken with quadrant vector grid at 200 v net accelerating potential and 6.6 ma beam current.

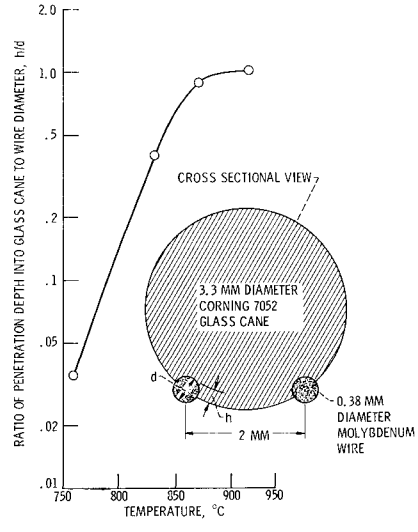

Fig. 12 Ratio of penetration depth into glass cone as a function of temperature for a 1-hr heating period.

Table 1 System performance of 5-cm thruster

	Data			Projection	
	1	2	3	4	5
Beam power, w	13.5	19.5	19.5	19.5	30.0
Accel. drain, w	0.14	0.20	0.18	0.2	0.45
Discharge, w	12.4	7.8	3.4	6.8	6.6
Cathode					
Keeper, w	4.6	4.6	7.0	3.5	3.5
Heater, w	15.0	15.0	16.4	7.0	7.0
Vaporizer, w	4.6	4.6	7.6	3.0	3.0
Neutralizer					
Keeper, w	3.36	3.36	3.36	3.0	3.0
Heater, w	9.4	9.4	9.4	5.0	5.0
Vaporizer, w	3.38	3.38	3.38	2.5	2.5
Total, w	66.4	67.8	70.2	50.5	61.1
Power efficiency	20.4	28.7	28.0	38.6	49.2
Prop. util. eff.	70	70	72	75	75
Over-all eff.	14.2	20.1	20	29	37
Beam current, ma	30	30	30	32	32
Thrust, mlb	0.30	0.36	0.36	0.36	0.44
I_{sp}, sec	1500	1800	1800	1800	2400
P/T, w/mlb	221	188	194	140	138

investigated. Operationally this concept is similar to the previous grid, except that vectoring would be accomplished in only one direction. Fabrication consisted of heating two 0.38-mm molybdenum wires that were kept in tension. Lengths of 3.3-mm-diam cane were placed on the two taut wires. By heating to various temperatures in a nitrogen environment it was possible to determine how much the wires would imbed themselves in the glass. Figure 12 shows a plot of the ratio of penetration depth into the glass cane to the wire diameter for various temperatures for one hour in a preheated oven. Slow cooling of these composite elements was necessary to prevent cracking. A completed grid made from 15 elements fired at 904°C was tested. Even though firing at this temperature resulted in a penetration depth about equal to the wire diameter, there still remained a strip of exposed molybdenum approximately 0.25-mm wide on each wire. The center-to-center spacing between canes was 5 mm. The ion extraction gap was 3 mm. Closer spacing was not possible because of a bulging at the ends of the glass cane. As a result, during testing, electron backstreaming occurred even at highly negative accelerator grid potentials. An improved design that also shadow shields the downstream surfaces from sputtered material is shown in Fig. 13. Fabrication techniques for this design are currently being investigated.

Another concept for thrust vectoring uses multiple electrodes bonded to a laminated insulator that contains multiple axisymmetric apertures. The grid consists of two 0.81-mm-thick glass sheets with conducting silver paint strips on each side of a rectangular array of holes. The holes were glass-bead-blasted through the glass using a drilled metal template. The silver conductor strips were painted on both sides of the downstream glass sheet. The upstream glass sheet shielded the downstream sheet from the ions in the discharge plasma.

A thruster test of this grid resulted in considerable electron backstreaming, which showed that smaller accelerator apertures and more substantial conductors are required.

Thruster System

The efficient and smooth operating component configurations were assembled for thruster system tests. Table 1 contains five columns of thruster system characteristics. The first three columns are data taken during thruster system tests. All data were taken with the same thruster at the same time with the exception of the neutralizer performance. The neutralizer data were taken on another thruster operating at the same beam current, extraction voltage, and propellant utilization efficiency as the thruster data in the respective column. The final two columns represent projected performance predictions. Hardware to evaluate these predictions is presently being fabricated. The major changes being made are to weld cathodes and vaporizers into single assemblies and to incorporate additional radiation shielding to minimize component heat losses. The projected columns list points at about 1800 and 2400 sec specific impulse. Reduced component size and improved discharge and extraction performance are longer range goals.

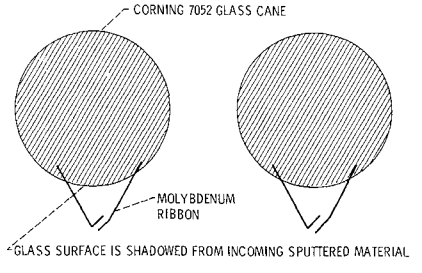

Fig. 13 Cross section of shadow shielded vector grid concept.

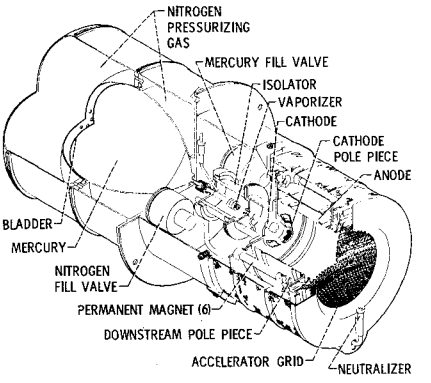

Fig. 14 5-cm electron bombardment thruster system.

Thruster data from Table 1 were used to size the propellant tankage for a rather arbitrarily defined 5-yr North-South station keeping requirement aboard a 1500-lb synchronous satellite. Incorporating all of the component characteristics into the system resulted in the design shown in the cutaway view of Fig. 14.

A positive expulsion single tank feed system operating at spacecraft potential supplies mercury to both the main and neutralizer cathodes. The nitrogen gas pressure in the volume surrounding the propellant tank deflects a hemispherical rubber bladder to keep liquid mercury in the main and neutralizer feed lines. Heated porous tungsten discs located in the lines vaporize the mercury at a controlled rate. Vapor from the main vaporizer flows through a high-voltage isolator and into the main cathode. The electrical isolator separates feed system components at spacecraft potential from those at thruster net accelerating potential. The mass of the thruster system shown in Fig. 14 is expected to be less than 2.1 kg. The tank holds 6.2 kg of mercury. Total impulses available with this propellant load range from 24,000 lb-sec at the demonstrated conditions of column 2, Table 1, to 33,000 lb-sec at the projected conditions of column 5.

Although attitude control and station keeping requirements for 1000–2000 lb synchronous spacecraft are the most immediate applications of the submillipound ion thruster, other uses are possible. The high total impulse capability on long duration missions can also be used to provide inertia wheel or control moment gyro momentum dump systems for high-pointing accuracy spacecraft such as orbiting or interplanetary observatory vehicles. The same high impulse capability and under 100 w power requirement may be of use as trajectory shaping propulsion on small (Radioisotope Thermionic Generator) powered outer planet probes and orbiters.

Concluding Remarks

A series of evaluation tests have been performed on components of 5-cm-diam electron bombardment ion thrusters. Power-to-thrust ratios of 190 w/mlb have been obtained at a

specific impulse of 1800 sec. The best over-all efficiency was 20% at a specific impulse of 1800 sec. It is estimated that simple thermal design cleanup of cathode and vaporizer units will allow operation at 140 w/mlb and 29% overall efficiency at 1800 sec. Preliminary testing with several electrostatic thrust vectoring concepts has resulted in the identification of some critical operational problems without a successful demonstration of beam vectoring. No fundamental barriers have been identified, however, and the investigation of electrostatic vectoring is proceeding.

References

[1] Boucher, R. A., "Electrical Propulsion for Control of Stationary Satellites," *Journal of Spacecraft and Rockets*, Vol. 1, No. 2, March-April 1964, pp. 164–169.

[2] Duck, K. I., Bartlett, R. O., and Sullivan, R. J., "Evaluation of an Ion Propulsion System for a Synchronous Spacecraft Mission," AIAA Paper 67-720, New York, 1967.

[3] Rawlin, V. K. and Kerslake, W. R., "SERT II: Durability of the Hollow Cathode and Future Applications of Hollow Cathodes," *Journal of Spacecraft and Rockets*, Vol. 7, No. 1, Jan. 1970, pp. 14–20.

[4] Banks, B. A., "A Fabrication Process for Glass Coated Electron-Bombardment Ion Thruster Grids," TN D-5320, 1969, NASA.

[5] Keller, T. A., "NASA Electric Rocket Test Facilities," *Seventh National Symposium on Vacuum Technology Transactions*, edited by C. R. Meisner, Pergamon Press, New York, 1961, pp. 161–167.

[6] Byers, D. C. and Staggs, J. F., "SERT II: Thruster System Ground Testing Performance," *Journal of Spacecraft and Rockets*, Vol. 7, No. 1, Jan. 1970, pp. 7–14.

[7] Margosian, P. M., "Preliminary Tests of Insulated Accelerator Grids for Electron Bombardment Thrustor," TM X-1342, 1967, NASA.

[8] Nakanishi, S., Richley, E. A., and Banks, B. A., "High-Perveance Accelerator Grids for Low-Voltage Kaufman Thrustors," *Journal of Spacecraft and Rockets*, Vol. 5, No. 3, March 1968, pp. 356–358.

[9] Lathem, W. C. and Staggs, J. F., "Divergent-Flow Contact-Ionization Electrostatic Thrustor for Satellite Attitude Control and Station Keeping," TN D-4420, 1968, NASA.

NOVEMBER 1970 J. SPACECRAFT VOL. 7, NO. 11

Aerodynamic Design of Axisymmetric Hypersonic Wind-Tunnel Nozzles

JAMES C. SIVELLS*
ARO Inc., Arnold Air Force Station, Tenn.

A unified approach to nozzle design is presented in which an inviscid contour is first determined and then corrected to account for the growth of a turbulent boundary layer along the contour. The inviscid contour is obtained by the axisymmetric method of characteristics from a prescribed distribution of velocity along the nozzle axis. The velocity distribution matches theoretical transonic conditions at the throat, conical-source flow conditions through an intermediate region, and design flow conditions at the nozzle exit. The second derivative of the axial velocity is continuous throughout and is zero at the exit point. The interdependence of some of the nozzle parameters is discussed. A semiempirical method is presented for calculating the boundary-layer correction. Calculated values agree within about 15% with experimental values obtained in 50-in.-diam, water-cooled nozzles over a Mach number range of 6 to 10.

Nomenclature

A^* = sonic area
a_e, a_0 = speed of sound at T_e and T_0, respectively
$B_{1,2}$ = coefficients in Eq. (73)
C_{1-4} = coefficients in Eq. (28)
C_f, C_{fi} = skin-friction coefficients, compressible and incompressible flow
D_{0-5} = coefficients in Eq. (37)
F_c $\equiv T'/T_e$
G_n = integrating factor for nth point
H = boundary-layer form factor, δ^*/θ
H_i = form factor, incompressible flow
K = square root of mass flow ratio
k $\equiv (\gamma + 1)/(\gamma - 1)$
M = Mach number
R = ratio of throat radius of curvature to throat radius
R_1 $\equiv r_1/r^*$
R_{x_e} = freestream Reynolds number based on x
R_θ, R_{θ_i} = compressible and incompressible Reynolds numbers based on momentum thickness
r = radial distance from source
r_1 = value of r when $M = 1$
r^* = radius of geometric throat
S $\equiv R + 1$
s $\equiv x_{n-1} - x_{x-2}$
T, T_s = static and stagnation temperatures within boundary layer
T_{aw} = adiabatic wall temperature
T_e, T_0 = freestream static and stagnation temperatures
T_w = wall temperature
T' = reference temperature
t $\equiv x_n - x_{n-1}$
U, U_e = transformed velocities within and at edge of boundary layer
u, u_e = velocities within and at edge of boundary layer
W = (velocity)/(velocity at sonic point)
X_E $\equiv (x_E - x_I)/r_1$
x = axial distance from source [except Eqs. (12, 14, and 17)]
Y = transformed distance normal to surface
y = distance normal to axis
α = factor in Eq. (62)

Presented as Paper 69-337 at the AIAA 4th Aerodynamic Testing Conference, Cincinnati, Ohio, April 28–30, 1969; submitted May 14, 1969; revision received August 17, 1970. The research reported herein was sponsored by the Arnold Engineering Development Center, Arnold Air Force Station, Tenn., under Contract F40600-70-C-0001 with ARO, Inc. Reproduction to satisfy the needs of the U.S. Government is authorized.

* Staff Engineer, Aerodynamics Division, von Kármán Gas Dynamics Facility. Associate Fellow AIAA.